ELSEVIER

Journal of Physics and Chemistry of Solids 64 (2003) 185–192

JOURNAL OF PHYSICS AND CHEMISTRY OF SOLIDS

www.elsevier.com/locate/jpcs

Pressure induced transitions in calcium: a tight-binding approach

G.M. Wang[a], D.A. Papaconstantopoulos[a,b], E. Blaisten-Barojas[a,*]

[a]*School of Computational Sciences, George Mason University, Fairfax, VA 22030, USA*
[b]*Center for Computational Materials Science, Naval Research Laboratory, Washington, DC 20375, USA*

Received 21 November 2001; accepted 20 February 2002

Abstract

A tight-binding (TB) hamiltonian for calcium is built with a high precision parametrization technique based on density functional calculations of the energy bands and the total energy at various lattice volumes. The new set of TB parameters is appropriate to study phenomena under pressures as high as 20 GPa. Specifically, both the metal to nonmetal transition at 4 GPa and the structural transition fcc to bcc at 19 GPa are well reproduced. These transitions and several static properties are in excellent agreement with experiments. Phonon frequencies, plasmon energy, melting temperature and the coefficient of thermal expansion were calculated with a molecular dynamics scheme of this TB hamiltonian.

PACS: 71.20. − b; 71.30. + h; 83.10.Tv; 65.40.De

1. Introduction

One of the interesting characteristics of alkaline-earth metals is their behavior under pressure. Calcium and strontium undergo a structural transition from fcc to bcc when high pressure is applied while the opposite is observed in other metals. Alkaline-earth metals are much softer than the transition metals or noble metals. Additionally, the mechanical properties of the various alkaline-earths are notably different from other metals as demonstrated by experiments under pressure [1–4]. In strontium, the structural transition from fcc to bcc takes place at 3.5 GPa whereas in calcium it is observed at 19 GPa when the volume is reduced by about 50% [1,3]. At lower pressures, both calcium and strontium display a metal–nonmetal transition in which the metallic character is lost. This transition is characterized by a gap in the density of electronic states (DOS) at the Fermi energy. Because of this phenomenon, calcium and strontium are known to be semimetals. Altmann and Cracknell [2] first predicted this anomaly in the electrical conductivity of calcium shortly before the metal–nonmetal transition was observed experimentally [1].

Theoretically the metal–nonmetal transition in calcium was studied within the augmented plane wave (APW) method [5,6]. These authors were able to locate the nonmetal state of calcium through a careful calculation of the DOS at the Fermi level, which was found to be almost zero at a pressure close to 5 GPa. In 1974, Mickish et al. [7] used a linear combination of localized atomic-orbitals within the density functional formalism to calculate the electronic bands of calcium and essentially duplicated the APW results [6] by confirming the metal–nonmetal transition. The structural transition fcc to bcc was not addressed in these studies. For calcium this transition was first analyzed within the frame of total energy calculations using a full potential linearized APW approach (LAPW) [8]. Years later the study was carefully revisited [9] by obtaining the Bain path or continuous shape deformation of the fcc unit cell into the bcc unit cell within the LAPW scheme.

In this work, we are interested in obtaining a set of parameters for the tight-binding (TB) hamiltonian of calcium that would allow a correct description of properties under high pressures. TB offers the possibility to study a wide range of material properties with a considerably less expensive computational investment than any density functional approach. However, the parametrization of this model is crucial to adequately reproduce the desired phenomenon. At present there is no set of TB parameters that would allow a good representation of the calcium properties

* Corresponding author. Tel.: +1-703-993-1988; fax: +1-703-993-1993.
E-mail address: blaisten@gmu.edu (E. Blaisten-Barojas).

0022-3697/03/$ - see front matter © 2002 Elsevier Science Ltd. All rights reserved.
PII: S0022-3697(02)00199-3

under high pressures. The best existing TB parameters [10] are appropriate for studying the properties under normal conditions but fail at high pressures.

Our strategy for finding the TB parameters for calcium is to fit them to density functional results of the band structure and total energy of both fcc and bcc lattices at different lattice constants. This is the strategy that has been followed in the NRL-TB method [10]. In this work, we extend the validity of the TB parametrization for calcium given in Ref. [10] by expanding the range of lattice constants to be commensurate with pressures at which the density of the material is increased by a factor of two. This extension provides the capability to further explore dynamical properties of calcium under pressure using TB molecular dynamics (TBMD) and to explore thermodynamic and mechanical properties not attainable earlier. To implement our strategy, we performed APW calculations of the energy bands and total energy of both fcc and bcc lattice structures for a wide range of lattice constants. These calculations include a soft-core scheme that considers the $3p^6$ electrons as valence electrons. Results from our first principles calculations are in agreement with earlier studies [6,9], although we report in this work a more precise value of the transition pressure for both the metal–nonmetal transition and the structural transition from fcc to bcc.

The organization of this paper is as follows. In Section 2 a description of the NRL-TB model is provided with a summary of the APW calculations. Comparison of energy bands and total energy obtained with both methods using the new parametrization is given in Section 3. The elastic properties at normal conditions are also described in Section 3. Section 4 provides results concerning the metal–nonmetal transition and the fcc to bcc structural transition obtained with the newly parametrized TB and with APW. Section 5 describes the TBMD calculation of several dynamical quantities such as the mean square displacement as a function of temperature, the thermal expansion coefficient and the phonon frequencies at selected points in the irreducible Brillouin zone (IBZ).

2. The tight-binding parametrization for calcium

Density functional calculations on calcium were carried out with the APW method in the muffin-tin approximation. This approximation is very reliable for cubic structures. At high pressures when the volume of the unit cell is compressed up to 50%, it is crucial to consider the 3p electrons as valence electrons. Here we used the Hedin–Lundqvist [11] prescription for exchange and correlation potential. These calculations were performed using 89 and 55 k-points in the IBZ for fcc and bcc crystals, respectively. For the calculation of the fcc DOS we used a grid of 505 k-points in the IBZ to determine precisely the values of the Fermi energy E_F. The APW total energy and electronic band results are then used to derive TB parameters by a nonlinear least square fit [10].

The NRL-TB method is based on the Slater–Koster (SK) approach [12] and is described in Refs. [10,13]. This scheme includes s, p and d atomic orbitals to form a 9×9 matrix representation of the TB hamiltonian. The k-independent parts of the SK hamiltonian matrix elements are considered as parameters. Due to the symmetry of the atomic orbitals, the number of distinct parameters in the SK hamiltonian is reduced to four on the diagonal and ten nondiagonal matrix elements per neighbor. In our work, we used a nonorthogonal basis set of atomic orbitals [14]. For this case the nondiagonal terms of the overlap matrix increase the number of SK parameters to 24. This approach is more desirable since it provides a larger number of parameters for fitting the energy bands and total energies. The diagonal elements of the SK hamiltonian are known as the on-site integrals s, p, t_{2g} and e_g. The nondiagonal terms of the SK hamiltonian are the hopping integrals ssσ, spσ, ppσ, ppπ, sdσ, pdσ, pdπ, ddσ, ddπ and ddδ.

In the standard SK scheme the on-site, hopping and overlap integrals are designated according to the atomic neighborhood considered in a specific calculation (first, second or third neighbors) [14]. The advantage of the NRL-TB method resides in these integrals being approximated by functionals of the intersite distances R_{ij} from one atom at site i to atoms within the lattice located inside a large sphere centered at that specific atom. The SK integrals become environment dependent. The on-site integrals are

$$O_l(\rho) = \alpha_l + \beta_l \rho^{2/3} + \gamma_l \rho^{4/3} + \delta_l \rho^2 \tag{1}$$

where l is a running index identifying the four different integrals. The quantities α_l, β_l, γ_l and δ_l are parameters to be fitted, and ρ is the local atomic density around each atom i in a given lattice structure

$$\rho_i = \sum_{j \neq i} \mathrm{e}^{-\lambda^2 r_{ij}} F_c(R_{ij}) \tag{2}$$

Here λ is a parameter to be fitted and the cutoff function defining the spatial range of every SK integral is

$$F_c(R) = \frac{1}{1 + \mathrm{e}^{2(R-R_0)/R}} \tag{3}$$

where $R_0 = 31$ a.u. such that 19 shells around every atom are included in the case of the fcc lattice and 25 shells in the case of the bcc lattice. Therefore, a radius of 34 a.u. for interactions around each atom is ensured, considerably larger than the typical value for transition metals of 16.5 a.u. [10]. This choice was made due to the fact that calcium has a much larger lattice parameter than the transition metals.

The 10 hopping integrals and the 10 nondiagonal elements of the overlap matrix are expressed as polynomials of the intersite distance R

$$H_m(R) = (a_m + b_m R + c_m R^2)\mathrm{e}^{-d_m^2 R} F_c(R) \tag{4}$$

Table 1
TB parameters in Eqs. (1) and (4). The parameter in Eq. (2) is $\lambda = 1.146303$. Units are Bohr for distances and Ry for energies

On-site		α	β	γ	δ
	s	0.047454	10.624	−524.24	18204
	p	0.13165	43.364	−1581.2	26017
	t_{2g}	0.15103	5.5955	−9.2518	−1437.5
	e_g	0.15103	5.5955	−9.2518	−1437.5
Hopping		a	b	c	d
	ssσ	111.77	−16.812	−1.5181	1.041
	spσ	−5.3099	1.4725	−0.0069709	0.77799
	ppσ	−12.263	0.84196	0.35675	0.82343
	ppπ	20683	−1110.3	−372.56	1.4587
	sdσ	1.1854	−0.3931	0.024818	0.61351
	pdσ	8.9528	−1.4176	−0.079699	0.82313
	pdπ	0.33013	−0.023055	-3.4477×10^{-4}	0.56197
	ddσ	−35.701	14.191	−1.5885	0.9379
	ddπ	−2.8139	1.0469	−0.061129	0.75552
	dδ	−1247.1	611.7	−71.613	1.2531
Overlap	ssσ	7.4856	−0.82752	2.9023×10^{-3}	0.6591
	spσ	44090	−8673.5	24.78	1.3096
	ppσ	57.107	−24.3	1.995	0.87409
	ppπ	647.98	−32.747	0.17389	1.2207
	sdσ	−175.12	27.776	1.6147	0.98484
	pdσ	−38.525	11.817	−0.8192	0.80281
	pdπ	−5.6075	0.40331	−0.076214	0.87489
	ddσ	−4.151	1.549	−0.084458	0.76831
	ddπ	−52850	18197	−1607	1.3065
	ddδ	7.028×10^5	-2.0927×10^5	15490	1.5242

where m is a running index identifying the 20 different integrals of the hamiltonian and overlap matrices. In this expression a_m, b_m, c_m and d_m are parameters to be fitted.

Under this scheme we fitted 97 parameters entering in Eqs. (1), (2) and (4) to the energy bands and total energy of 13 lattice structures: eight fcc calculations with lattice constants ranging from 8.0 to 11.5 a.u., and five bcc structures with lattice constants ranging from 7.2 to 8.4 a.u. A nonlinear fit yielded an rms-error of 0.5 mRy for the total energy of the 13 structures. The corresponding error on the six lowest energy bands of each of the 13 lattice structures ranged between 9 mRy for normal volumes and 18 mRy for the highly compressed fcc structure. Table 1 contains all fitted parameters. Worth noting is that several SK hopping integrals are quite long-range functions. For example, spσ, ppσ and pdσ have significant values even at $R = 16$ a.u.

It should be pointed out that when calculating the total energy and energy bands with APW, we used the scheme in which pseudo-one-electron states are defined under the following prescription. The total electron energy of the solid in terms of the electron density $n(\vec{r})$ is

$$E[n(\vec{r})] = 2\sum_i f(E_F - \epsilon_i)\epsilon_i + G[n(\vec{r})] = 2\sum_i f(E_F' - \epsilon_i')\epsilon_i' \tag{5}$$

where ϵ_i are the Kohn–Sham eigenvalues, G contains the remaining terms depending on $n(r)$ and E_F is the Fermi energy. The summation runs over all electron states such that their occupation number $f(E_F - \epsilon_i)$ satisfies the sum rule

$$N_e = 2\sum_i f(E_F - \epsilon_i) \tag{6}$$

with N_e being the number of electrons in the system. Pseudo-eigenvalues ϵ_i' are defined by

$$\epsilon_i' = \epsilon_i + G[n(\vec{r})]/N_e \tag{7}$$

and the total energy is then expressed as a sum of one-electron pseudo-eigenvalues as shown in Eq. (5). This expression is simpler to compare to the TB total energy description. The energy bands on which the fit of the TB parameters was carried out were built with these pseudo-eigenvalues.

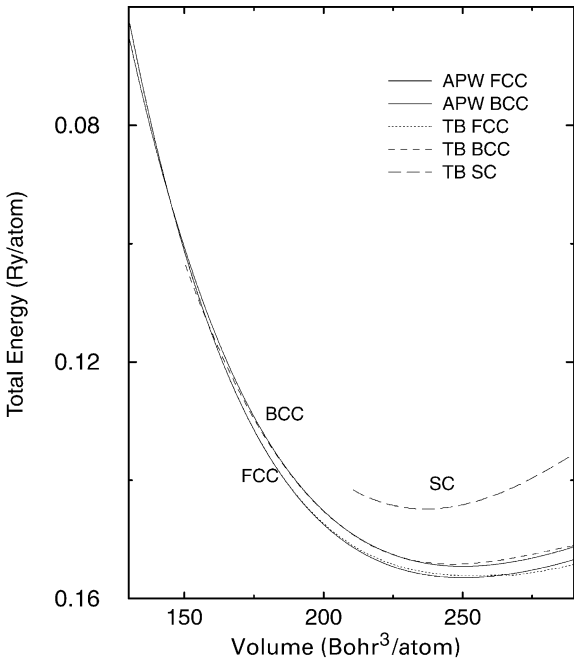

Fig. 1. Total energy vs. unit cell volume. Solid curves are APW calculations (fcc and bcc). Dotted (fcc), dashed (bcc) and long-dashed (sc) are TB calculations.

3. The tight-binding total energy and energy bands of calcium

Fig. 1 shows the total energy as a function of the unit cell volume for fcc, bcc and simple cubic (sc) structures. Solid curves illustrate the APW calculations and dashed lines correspond to the TB energies. As is typical in the local density approximation, the calculated equilibrium lattice constant $a_0 = 9.98$ a.u. is smaller than the experimental value of 10.54 a.u. The TB value is $a_0 = 10.11$ a.u.. The figure shows clearly that the TB parametrization is in excellent agreement with APW in a wide range of unit cell volumes. The previous TB parametrization [10] breaks down at volumes of about 170 a.u. As a proof of the robustness of our TB hamiltonian, Fig. 1 shows the total energy curve of the sc lattice. As expected, the energy of this structure is far above the fcc and bcc energies.

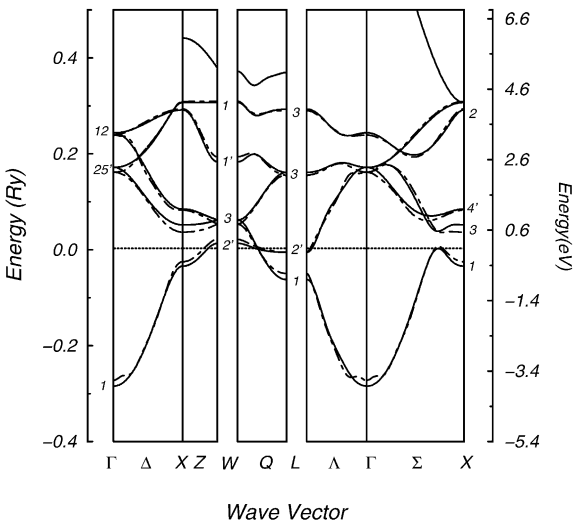

Fig. 2. Energy bands for the fcc lattice with $a = 10.54$ a.u. Solid lines are APW results and dashed lines are the TB results. The Fermi level is shifted to zero.

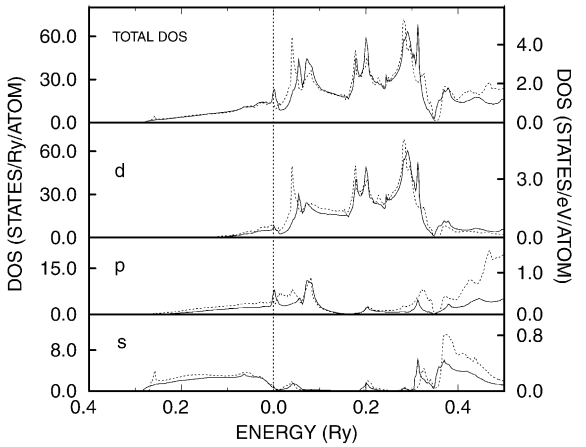

Fig. 3. Density of states for the fcc lattice with $a = 10.54$ a.u. Solid lines stand for APW calculations and dotted lines for the TB calculation. The Fermi level is shifted to zero.

Energy bands and DOS for the fcc lattice at the experimental lattice constant are plotted in Figs. 2 and 3 where the Fermi energy has been shifted to zero. Our TB parametrization gives excellent agreement with the APW results on both the energy bands and the DOS as seen from the figures. Specifically, the TB occupied band width $E_F - E(\Gamma_1)$ (mostly s character) is 283 mRy. The d band width $E_{W_1} - E_{W_3}$ is 252 mRy. Bandwidths are very clearly seen in the decomposition of the DOS plotted in Fig. 3. These widths are in excellent agreement with the corresponding APW values of 286 and 243 mRy, as well as with the experimental value of 285 mRy for the width of the occupied band [15]. The correlation energy is fundamental when determining these bandwidths. For such reason the agreement between APW and experiment for the bandwidth of the occupied band is excellent. Both TB and APW display comparable DOS at the Fermi energy $N(E_F)$ of about 21 and 20 states/Ry/atom, respectively.

Using the values of $N(E_F)$ at equilibrium (10.4 states/Ry/atom for TB and 12 states/Ry/atom for APW) the TB estimate of the electronic specific heat coefficient is 2.2 mJ/mol/K^2 to be compared with 2.9 mJ/mol/K^2 from both APW and experiment with an enhancement factor of 1.39 [14].

The comparison of our TB and the APW energy bands

Table 2
Elastic constants and their comparison with experiments and other calculations

	B (GPa)	$C_{11}-C_{12}$ (GPa)	C_{11} (GPa)	C_{12} (GPa)	C_{44} (GPa)
This work (TB)	17.2	8.3	22.7	14.4	21.0
Experiment [17]	21.4	9.6	27.8	18.2	16.3
Experiment [18]	10.7	8.0	16.0	8.0	12.0
Ref. [19]	12.0	7.0	16.7	9.7	14.2

and DOS holds extremely well at compressed unit cell volumes consistent with high pressures. For example, the TB bandwidths of the occupied band and of the d band are 338 and 337 mRy at 4 GPa. These values change to 341 and 423 mRy at 19 GPa. The corresponding APW bandwidths are 324, 326 mRy at 4 GPa and 344, 405 mRy at 19 GPa showing the excellent agreement of TB with APW energy bands.

Generic similarities between the energy bands of calcium and ytterbium are often cited in the literature. However, we note that while the spin–orbit coupling in ytterbium removes the accidental degeneracy of the first and second bands along the WQL direction of the IBZ [16], for calcium the degeneracy is not lifted because the spin–orbit coupling is too weak. The latter statement is supported by calculations at various pressures where we extended the APW approach to include spin–orbit coupling with a spin–orbit coupling constant of 1 mRy.

Elastic properties are listed in Table 2 for the fcc lattice at the experimental lattice constant. As seen from these results, the TB values compare very well to the experimental bulk modulus and $C_{11} - C_{12}$ constants. The individual calculated values of C_{11}, C_{12} and C_{44} are not as close to experiment as desired. However, this is not surprising for a metal as soft as calcium for which there is no agreement even between different experiments [17,18]. Since experimentally only three elastic constants are reported, the relation $B = (C_{11} + 2C_{12})/3$ was used to obtain the bulk modulus. Only a full representation of the valence electron potential such as in LAPW rather than the muffin-tin description of APW improves the calculated values of C_{44}. The table includes published results obtained with LAPW [19].

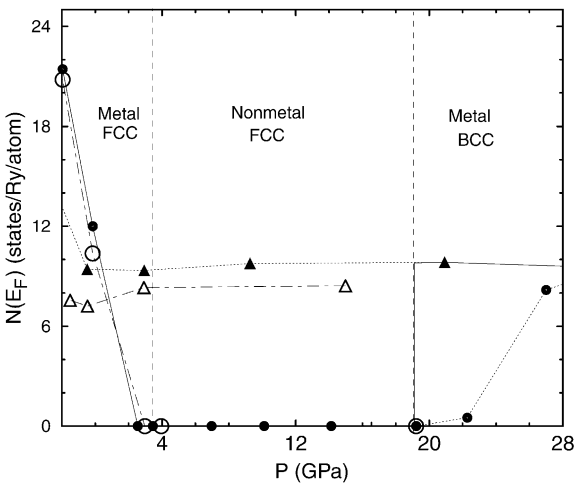

Fig. 4. Density of states at the Fermi energy vs. pressure. APW fcc (black circles), APW bcc (black triangles), TB fcc (open circles), and TB bcc (open triangles).

4. The metal–nonmetal transition and the structural transition

The signature of a metal is its DOS at the Fermi energy $N(E_F)$. Under pressure, the $N(E_F)$ of calcium steadily decreases to reach zero around 4 GPa, whereas the most stable lattice structure continues to be fcc. This characteristic identifies the material as a semimetal in which a metal–nonmetal transition occurs when the material is driven away from normal pressure and density. Based on finding the pressure at which $N(E_F)$ becomes zero, both our TB and APW approaches predict a transition pressure of 4 GPa. Here the pressure is calculated from

$$P - P_0 = -\int_{V_0}^{V_{\text{desired}}} \frac{\partial^2 E(V)}{\partial V^2} \mathrm{d}V \tag{8}$$

where V stands for the volume of the unit cell and V_0 is this volume at equilibrium of the total energy $E(V)$ depicted in Fig. 1 for either the fcc or bcc lattices. At V_0, the pressure is $P_0 = 0$.

The phase portrait in the $N(E_F)$–P plane shown in Fig. 4 summarizes our results. Increasing the pressure above normal pressure to about 4 GPa we observe that $N(E_F)$ is larger than zero for the fcc lattice reassuring the metallic character of calcium (black dots are APW and circles are TB). However, above 4 GPa the $N(E_F)$ remains zero up to about 19 GPa. In contrast, the $N(E_F)$ of the bcc lattice is basically constant in this pressure domain (black triangles are APW and white triangles are TB). A clear distinction of two regions, below and above 4 GPa highlights the metal nonmetal transition.

In earlier APW calculations [6] the search was not as extensive and a transition pressure of 5 GPa was estimated. Experimentally, the transition is reported in terms of the ratio between the lattice constant at a given pressure and the lattice constant at normal pressure. The experimental ratio a/a_0 at the transition is 0.875 [1]. Our value of 0.896

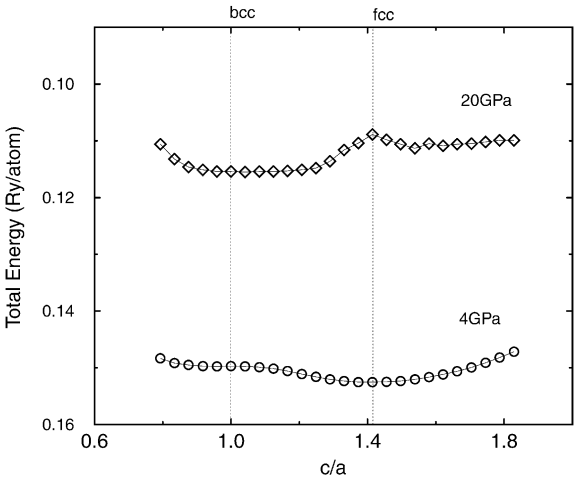

Fig. 5. Bain-path at two different pressures.

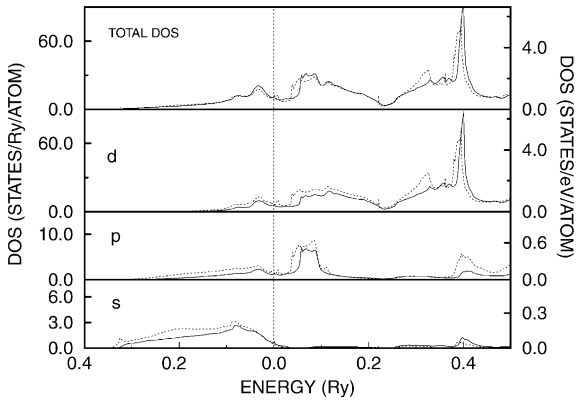

Fig. 7. Density of states of the bcc lattice at 15.2 GPa ($a = 6.973$ a.u.). Solid lines are APW results and dotted lines are TB results.

differs by 2.4%. Other studies have reported similar estimates for this ratio: 0.93 [6], 0.82 [7], 0.943 and 0.866 [20].

As pressure is increased beyond 19 GPa the fcc lattice is no longer the most stable structure but rather deforms steadily into the bcc lattice. Inspection of the phase portrait of Fig. 4 shows that in addition to the structural transition, there is a discontinuous change in $N(E_F)$ from zero to about 9 states/Ry/atom at about 19 GPa. Therefore, at this pressure calcium clearly undergoes a transition to the bcc structure as well as to a metallic state. Our conclusion is in agreement with the most recent experiments [4] and earlier calculations [9]. Fig. 5 shows TB results at two relevant pressures of the Bain deformation path in which a body-centred tetragonal unit cell with lattice constants a, c continuously deforms as the ratio c/a changes. When $c/a = 1$ the structure is bcc and when $c/a = \sqrt{2}$ the lattice is fcc. As seen in Fig. 5, at 4 GPa where calcium is nonmetallic, the Bain path has its minimum at the fcc lattice. At 20 GPa the bcc lattice structure becomes a minimum and calcium is metallic again. To produce Fig. 5, a mesh of 322 k-points in the IBZ was used. Our TB results are in good agreement with previous LAPW results [9].

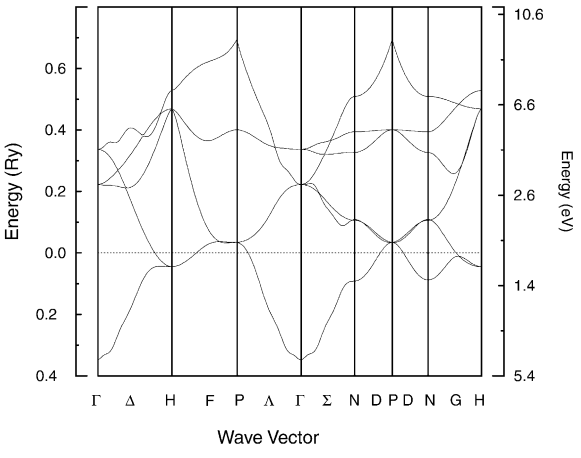

Fig. 6. Energy bands of the bcc lattice at 15.2 GPa within TB.

In Figs. 6 and 7, the bcc TB energy bands and DOS (APW and TB) are shown for bcc calcium under 15 GPa ($a = 6.973$ a.u.). At this pressure the volume of calcium is compressed to almost half the normal volume. The compressed lattice structure for these two figures is different than any of the compressed bcc structures used in the fit of the TB parameters showing the transferability of the TB hamiltonian. The bcc energy bands are quite stiff although increases in pressure still enlarge the bandwidths. For example, the width of the occupied band is increased from 311 to 345 mRy when pressure is increased by 15 GPa. The TB DOS compares very well to APW results even at these compressed volumes. Therefore, the crucial change at the structural transition pressure of 19 GPa is the dramatic transition from the nonmetallic state in which calcium is fcc to the metallic state in which calcium becomes bcc under higher pressures.

Implications of these pressure induced transitions impact other properties such as the Drude plasmon energy. The plasmon frequency $\Omega_p^2(E_F) = (4\pi/3)e^2N(E_F)v^2(E_F)$ ($v(E_F) =$ velocity at E_F) presents a sharp pressure dependence. At the equilibrium fcc volume the calculated plasmon energy is 1.8 eV (APW) and 1.9 eV (TB). This energy remains zero between 4 and 19 GPa while the material is nonmetal and acquires a value of 4.0 eV when the crystal undergoes the structural transition to bcc. The decomposition of the DOS in the various symmetry components is also of interest. At low pressures the main contribution to $N(E_F)$ is given by both the p and d-like states which contribute by 50 and 46%, respectively. At pressures above the structural transition, when the material is bcc, the contribution of d states is about 73% whereas the p-like states contribute only 17% and the remaining states are s-like.

Table 3
Phonon frequencies at high symmetry points of the IBZ

k		Frozen phonon (THz)	TBMD (THz)	Experiment [17] (THz)
Δ	L	4.76	4.61	3.66
	T	3.81	2.61	2.54
X	L	8.20	8.03	4.52
	T	5.30	5.23	3.63
L	L	4.51	4.16	4.61
	T	3.33	2.79	2.36

5. Tight-binding molecular dynamics simulations

The TB model has been coupled with molecular dynamics (TBMD) in various different schemes. In this work, we adopted the implementation put forward by Kirchhoff and co-workers [21]. The ionic equations of motion were solved within the velocity form of the Verlet algorithm with a time step of 1.5 fs. All calculations were performed with computational cells containing 108 atoms, consistent with the fcc lattice unit cell translated three times in each cartesian direction.

At normal temperature and pressure, we calculated dynamically the longitudinal (L) and transverse (T) phonon frequencies at the symmetry points Δ, X and L of the IBZ. The velocity autocorrelation function as a function of the position of each lattice site in the unit cell was obtained such that peaks of its Fourier transform identified the desired phonon frequencies. Table 3 reports our results. Additionally, we obtained static estimates of these same frequencies within the frozen phonon scheme [22]. Frequency estimates and the experimental values from neutron diffraction [17] are contained in the same table. The Δ and L modes are in very good agreement with experiment. However, the X modes are systematically higher close to the IBZ edge. We believe that this discrepancy is related to the lack of ability that TB displays to reproduce the C_{44} elastic constant and to the small number of atoms considered in our calculation.

Following the Lindemann criterion [23] to estimate the melting temperature, we calculated the mean square displacement (MSD) of calcium atoms in the fcc lattice at normal density and at temperatures ranging from 290 to 1200 K. The MSD averages increase smoothly as a function of increasing temperature. At about 1180 ± 120 K the MSD average is about 15% of the nearest distance in the fcc lattice. At this temperature, according to Lindemann criterion, the calcium fcc lattice undergoes melting. Our estimate is in excellent agreement with the experimental value of 1115 K [24]. The error we report for the average associated to the temperature corresponds to twice the standard deviation.

The linear thermal expansion coefficient defined by

$$\alpha = \frac{1}{3V}\left(\frac{\partial V}{\partial T}\right)_{P_0} \tag{9}$$

was also calculated at normal pressure P_0. This requires MD simulations for several densities at a given temperature. For each unit cell volume V the average pressure $P(V)$ was computed at various temperatures between 300 and 600 K to identify the volume V_1 at which the pressure is 1 atm. As a second stage, we choose a volume V_2 slightly larger than V_1 and calculate the average pressure at various temperatures between 300 and 600 K. Interpolation of these values gives a linear $P_0(T)$ dependence from where α is estimated as $(15 \pm 7) \times 10^{-6}\,\mathrm{K}^{-1}$. The experimental value is $21 \times 10^{-6}\,\mathrm{K}^{-1}$ [24]. The agreement is reasonable considering that calcium is a very soft metal.

6. Conclusions

In this paper we have generated a new set of TB parameters that allow to study the properties of calcium at pressures as high as 20 GPa and temperatures above 1500 K. Previous parametrizations only permitted studies close to normal thermodynamic conditions. We have shown that the new TB model reproduces well the metal nonmetal transition at 4 and 19 GPa describes correctly the structural transition fcc to bcc in which the material becomes metallic again. The elastic properties, electronic specific heat, phonon frequencies, and melting behavior obtained with the new TB model are all in very good agreement with experimental observations. The TB hamiltonian constructed in this work is expected to apply in other problems such as in the validation of many-body potentials [25,26].

The findings of this work for alkaline-earth interactions carry over to other length scales. The long range character of the calcium–calcium forces added to a very hard core is a characteristic responsible for the peculiar cluster growth sequence that has been predicted for both calcium and strontium [25,27]. For example, Ca_{13} is a twinned pentagonal bipyramid with two capped faces. This is a very different

structure than the icosahedron obtained for most metals. The long range characteristic of the interactions are also responsible for the softness of these alkaline-earth metals.

Acknowledgements

E.B.B. acknowledges partial support from Grants CTS-9806321 of the National Science Foundation and N00014-98-1-0832 of the Office of Naval Research. G.M.W. wishes to thank Dr M.J. Mehl for useful discussions.

References

[1] R.A. Stager, H.G. Drickamer, Phys. Rev. 131 (1963) 2524.
[2] S.L. Altmann, A.P. Cracknell, Proc. Phys. Soc. 84 (1964) 761.
[3] A.A. Bakanov, I.P. Dodoladov, JETP Lett. 5 (1967) 265.
[4] H. Olijnyk, W.B. Holzapfel, Phys. Lett. A 100A (1984) 191.
[5] J.W. McCaffrey, D.A. Papaconstantopoulos, J.R. Anderson, Solid State Commun. 8 (1970) 2109.
[6] J.W. McCaffrey, J.R. Anderson, D.A. Papaconstantopoulos, Phys. Rev. B 7 (1973) 674.
[7] D.J. Mickish, A.B. Kunz, S.T. Pantelides, Phys. Rev. B 10 (1974) 1369.
[8] R.M. Wentzcovich, H. Krakauer, Phys. Rev. B 42 (1990) 4563.
[9] V.L. Sliwko, P. Mohn, K. Schwarz, P. Blaha, J. Phys.: Condens. Matter 8 (1996) 799.
[10] M.J. Mehl, D.A. Papaconstantopoulos, Phys. Rev. B 54 (1996) 4519.
[11] L. Hedin, B.I. Lundquist, J. Phys. C 4 (1971) 2064.
[12] J.C. Slater, G.F. Koster, Phys. Rev. 94 (1954) 1498.
[13] R.E. Cohen, M.J. Mehl, D.A. Papaconstantopoulos, Phys. Rev. B 50 (1994) 14694.
[14] D.A. Papaconstantopoulos, Handbook of Electronic Structure of Elemental Solids, Plenum Press, New York, 1986 p. 23 and 63.
[15] K.A. Kress, G.J. Lapeyre, Solid State Commun. 9 (1971) 827.
[16] G. Johansen, A.R. Mackintosh, Solid State Commun. 8 (1970) 121.
[17] C. Stassis, J. Zaretsky, D.K. Misemer, H.L. Skriver, B.N. Harmon, R.M. Nicklow, Phys. Rev. B 32 (1985) 22.
[18] E.A. Brands (Ed.), Smithells Metals Reference Book sixth ed, Butterworths, London, 1983, pp. 15.2–6.
[19] M.J. Mehl, B.M. Klein, D.A. Papaconstantopoulos, in: J.H. Westbrook, R.L. Fleischer (Eds.), Intermetallic Compounds: Principles and Applications, vol. 1, Wiley, London, 1994, p. 195.
[20] S. Asano, J. Yamashita, J. Phys. Soc. Jpn 35 (1973) 767.
[21] F. Kirchhoff, M.J. Mehl, D.A. Papaconstantopoulos, F.S. Khan, Phys. Rev. B 63 (2001) 195101.
[22] K.M. Ho, C.L. Fu, B.N. Hamon, W. Weber, D.R. Hamann, Phys. Rev. Lett. 49 (1982) 673.
[23] F.A. Lindemann, Z. Phys. 11 (1910) 609.
[24] Liele, D.R. (Ed.). Handbook of Chemistry and Physics, 81st ed., CRC Press, New York, 2001.
[25] G.M. Wang, E. Blaisten-Barojas, A.E. Roitberg, T.P. Martin, J. Chem. Phys. 115 (2001) 3640.
[26] C.H. Chien, E. Blaisten-Barojas, M. Pederson, J. Chem. Phys. 112 (2000) 2301.
[27] J.W. Mirick, C.H. Chien, E. Blaisten-Barojas, Phys. Rev. A 63 (2001) 23202.